



Published in final edited form as:

Nat Chem. 2022 December ; 14(12): 1421–1426. doi:10.1038/s41557-022-01048-2.

## Practical synthesis of the therapeutic leads tigilanol tiglate and its analogues

Paul A. Wender<sup>1,2</sup>, Zachary O. Gentry<sup>1</sup>, David J. Fanelli<sup>1</sup>, Quang H. Luu-Nguyen<sup>1</sup>, Owen D. McAteer<sup>1</sup>, Edward Njoo<sup>1</sup>

<sup>1</sup>Department of Chemistry, Stanford University, Stanford, CA, USA.

<sup>2</sup>Department of Systems and Chemical Biology, Stanford University, Stanford, CA, USA.

### Abstract

Tigilanol tiglate is a natural product diterpenoid in clinical trials for the treatment of a broad range of cancers. Its unprecedented protein kinase C isoform selectivity make it and its analogues exceptional leads for PKC-related clinical indications, which include human immunodeficiency virus and AIDS eradication, antigen-enhanced cancer immunotherapy, Alzheimer's disease and multiple sclerosis. Currently, the only source of tigilanol tiglate is a rain forest tree, *Fontainea picrosperma*, whose limited number and restricted distribution (northeastern Australia) has prompted consideration of designed tree plantations to address supply needs. Here we report a practical laboratory synthesis of tigilanol tiglate that proceeds in 12 steps (12% overall yield, >80% average yield per step) and can be used to sustainably supply tigilanol tiglate and its analogues, the latter otherwise inaccessible from the natural source. The success of this synthesis is based on a unique strategy for the installation of an oxidation pattern common to many biologically active tiglanes, daphnanes and their analogues.

Ligands that modulate protein kinase C (PKC) signalling<sup>1</sup> have been implicated in therapeutic approaches to human immunodeficiency virus and AIDS eradication<sup>2</sup>, antigen-enhanced antibody and chimeric antigen receptor (CAR) T-cell therapies<sup>3,4</sup>, suppression of T-cell exhaustion in cancer immunotherapy<sup>5</sup>, Alzheimer's disease<sup>6</sup> and multiple sclerosis<sup>7</sup>.

Reprints and permissions information is available at [www.nature.com/reprints](http://www.nature.com/reprints).

**Correspondence and requests for materials** should be addressed to Paul A. Wender. [wenderp@stanford.edu](mailto:wenderp@stanford.edu).

#### Author contributions

Z.O.G., D.J.F., O.D.M., Q.H.L.-N. and E.N. prepared the compounds; D.J.F. performed the binding and translocation assays; E.N. performed the computational studies; P.A.W. and all the authors provided guidance on the design and analysis of experiments and wrote the manuscript.

#### Competing interests

A provisional patent application (docket number S21-064) has been filed by Stanford University, on behalf of Paul A. Wender (principal investigator), Zachary O. Gentry, David J. Fanelli, Quang H. Luu-Nguyen, Owen D. McAteer and Edward Njoo, that covers a method to synthesize tigilanol tiglate (EBC-46) and related compounds from readily available starting materials.

**Supplementary information** The online version contains supplementary material available at <https://doi.org/10.1038/s41557-022-01048-2>.

#### Reporting summary

Further information on research design is available in the Nature Research Reporting Summary linked to this article.

#### Online content

Any methods, additional references, Nature Research reporting summaries, source data, extended data, supplementary information, acknowledgements, peer review information; details of author contributions and competing interests; and statements of data and code availability are available at <https://doi.org/10.1038/s41557-022-01048-2>.

Some modulators have advanced towards clinical evaluation<sup>8,9</sup>, such as tigilanol tiglate (**1**, EBC-46), a naturally occurring tigliane diterpenoid recently evaluated in phase I clinical trials for the treatment of a broad range of cancers in humans and currently in trials for head and neck squamous cell carcinomas<sup>10</sup>. Intratumoural injection of EBC-46 induces rapid tumour ablation, in part by a proposed isoform-selective modulation of PKC<sup>11,12</sup>. After administration, EBC-46 induces a localized immune response and rupture of tumour vasculature, which leads to haemorrhagic necrosis, subsequent clearance of the solid tumour and facilitated wound healing<sup>13,14</sup>. Recently, EBC-46, branded Stelfonta, received approval by the US Food and Drug Administration<sup>15</sup> for the treatment of non-metastatic mast cell tumours in canines. In a recent clinical study, a 75% complete response was observed in canines after a single intratumoural injection and 88% remission after a second dose<sup>16</sup>, which prompted its current evaluation in human trials.

Currently, the only source of EBC-46 is the dioecious blushwood tree (*Fontainea picrosperma*), a rainforest *Euphorbiaceae*, limited in number and endemic to a small region of northeastern Australia<sup>17,18</sup>. As reported, to access EBC-46 and ester variants from rain forest tree seeds, the seeds are extracted with ethanol and the resultant extract is partitioned between petroleum ether and water. The contents of the organic phase are then converted into EBC-46 using six chromatographic purifications and five low-yielding synthetic steps (~5% yield)<sup>19</sup>. Prompted by its limited natural source, environmental considerations and its emerging clinical value, efforts to improve EBC-46 production have been directed at cultivating its source plant, *F. picrosperma*, in designed plantations<sup>17</sup>. However, this source, although it avoids rain forest harvesting, is still pollinator limited and at risk of disruption by climate variations and invasive pathogens<sup>18,20</sup>. More geographically distributed and diverse sources would offer a more sustainable supply for research and clinical needs.

Given the immediate clinical and research value of EBC-46 and its analogues, a practical and more sustainable solution to the supply problem could be realized through a time- and step-economical<sup>21</sup> semisynthesis from a more available and diversified source<sup>22</sup>. Similar strategies that combine the power of biological and chemical synthesis enable rapid access to other clinical candidates, such as Taxol and prostratin and their analogues<sup>22-26</sup>. Towards this end, phorbol esters represent potential precursors to EBC-46. Although available through total synthesis<sup>27-29</sup>, they are even more readily accessed from more than 7,000 species of the globally distributed *Euphorbiaceae* and *Thymelaeaceae* plant families<sup>30</sup>. Although plant cultivars vary in phorbol ester content, the seeds of the *Croton tiglium* plant of the *Euphorbiaceae* family supply upwards of 1.6% w/w of phorbol (**2**) upon extraction and ester hydrolysis<sup>31</sup>. Given the low cost (~US\$40 kg<sup>-1</sup>) of these seeds and the diverse geographical distribution of their varied sources, we set out to design a synthetic route to EBC-46 based on phorbol (**2**) as the starting material (Fig. 1). To obtain this material efficiently, we developed an improved scalable isolation protocol building on prior work<sup>32,33</sup> that, on average, afforded >10 g of phorbol (**2**) from 3 kg of seeds (Supplementary page SI-5). This isolation protocol consists of grinding the seeds and base-mediated removal of the C20, C12 and C13 esters in the extract to produce an oil from which phorbol (**2**) is purified by column chromatography.

A key challenge associated with synthetically accessing EBC-46 and many related, biologically active tiglane and daphnane natural products is the construction of their common B-ring 5 $\beta$ -hydroxy-6 $\alpha$ ,7 $\alpha$ -epoxy functionality (Fig. 2a)<sup>30,34</sup>. Based on our original pharmacophore model, we expect that this functionality, among other B-ring functional groups, influences PKC affinity, selectivity and function (Fig. 2b)<sup>35,36</sup>. Thus, the core of this problem is oxy-functionalization of the  $\beta$ -5 allylic hydrogen in the presence of other allylic hydrogens at C8, C20, C10 and C19. This problem is further exacerbated by phorbol's sensitivity to heat, light, acid, base and air oxidation<sup>37</sup>. Attempts at direct CH activation at C5 have thus far failed<sup>33,38</sup>. With a scalable source of phorbol (**2**) in hand, we now describe a solution to this problem that provides, in six steps, scalable access to a highly diversifiable intermediate **7** (Fig. 3) from which EBC-46 and new analogues are readily derived.

## Results and discussion

Anticipating that esters at C12 and C13 could be exchanged by late-stage diversification and would minimize interference with B-ring modifications, we opted to start with the simple diacetate **3**, which is prepared from phorbol (**2**) with an 82% yield via *t*-butyldimethylsilyl protection at C20 followed by acetylation at C12 and C13 and a desilylative workup (Fig. 3). Efforts to convert this two-step process into one step via triacetylation and selective deprotection of the C20 acetate gave lower yields (~65%) and was not utilized on large scale.

Chemo-, regio- and stereoselective oxidation at C5 of diacetate **3** in the presence of potentially oxidizable allylic sites at C8, C10, C19 and C20 was efficiently realized using a photosensitized singlet oxygen ene reaction with Rose bengal as the photosensitizer, green light-emitting diodes ( $\lambda = 535$  nm) as the photon source<sup>39,40</sup> and methanol-*d*<sub>4</sub> as the solvent, which minimizes singlet oxygen destruction<sup>40</sup>. In situ reduction of the resultant hydroperoxide initially produced allylic alcohol **4** in moderate yield (66%). Although this reaction can be routinely performed batch-wise on small scales (<500 mg), large-scale batch reactions suffered from light penetration issues and raised concerns about the accumulation of the potentially unstable hydroperoxide intermediate<sup>39</sup>. To address these scalability problems, we assembled a cyclic flow photoreactor that utilized a peristaltic pump and Tygon tubing (Supplementary Figs. 3 and 4)<sup>41</sup>. Using this apparatus, we produced the ene product **4** on a decagram scale (for example, 19 g) in an 88% yield as determined by quantitative NMR. Although further purified for characterization purposes, this compound was sufficiently pure to be used directly in the following step thereby avoiding chromatographic purification.

It was envisioned that **4** could be converted into the C5 alcohols **6** or **7** via rhenium-catalysed allylic transposition<sup>42,43</sup>. However, the reaction of **4** using literature conditions was sluggish and provided only minor amounts of the undesired C5 $\alpha$ -hydroxy-C6,C20 alkene. As an effective alternative route to **6**, we found that epoxidation of the C5,C6 alkene in **4** with *m*-chloroperbenzoic acid (*m*CPBA) proceeded preferentially from the sterically more accessible  $\beta$ -face to give epoxide **5**, with the desired C5 $\beta$ -O bond, in 77% yield. *N*-methylimidazole (NMI)-catalysed chemoselective tosylation of the primary C20 alcohol

and subsequent reaction with sodium iodide gave exclusively the desired  $\beta$ -C5 alcohol **6** in 88% yield<sup>44</sup>.

On treatment with catalytic Re<sub>2</sub>O<sub>7</sub>, the bis-allylic alcohol **6** underwent a highly chemoselective 1,3-allylic alcohol transposition<sup>42,43</sup> to afford C5 $\beta$ -hydroxy phorbol diacetate **7** in a 76% yield (90% based on recovered **6**), which serves as a diversification node<sup>21,24</sup> to access unexplored B-ring analogues of **1**. Other rhenium catalysts led to complex mixtures or a lower conversion (Supplementary Table 1).

Subsequent epoxidation of the C6,C7 alkene of **7** occurred only on the sterically more accessible (undesired)  $\beta$ -face, as expected from our previous work<sup>45,46</sup>. Although chiral catalyst-controlled epoxidation might address this selectivity problem<sup>46</sup>, we found a more effective solution; specifically, the facial selectivity exhibited by **7** can be dramatically reversed by the conversion of **7** into its acetonide **8** (92%). Models suggest that the acetonide between the C5 and C20 alcohols induces a conformational change in the B-ring that makes the  $\beta$ -face more sterically encumbered and the  $\alpha$ -face less so. Additionally, this protection of the C5 and C20 alcohols serves to simplify subsequent functionalization of the C12 and C13 alcohols. Although the initial epoxidation of acetonide **8** with *m*CPBA under a variety of conditions (Supplementary Table 2) was slow and low yielding, we found that treatment with the sterically smaller and more reactive dimethyldioxirane (DMDO) stereoselectively gave  $\alpha$ -epoxide **9** in a 63% yield. This substrate-controlled facially selective epoxidation is unprecedented for this class of compounds and thus provides a potentially general method to access other structurally similar and biologically active tiglane and daphnane diterpenoids<sup>30,34</sup>.

Deacetylation of diester **9** provided the corresponding C12,C13 diol **10** in an 86% yield as determined by quantitative NMR. Although further purified for characterization purposes, this compound was sufficiently pure to be used directly in the following step thereby avoiding chromatographic purification. Diol **10** serves as a second point of diversification for C12,C13 derivatization, now with the desired C5 $\beta$ -hydroxy-C6 $\alpha$ ,C7 $\alpha$ -epoxy B-ring in place<sup>11,24,36</sup>. From **10**, EBC-46 was prepared on gram scale via selective diesterification<sup>47</sup> and acidic deprotection of the acetonide. In our laboratory, this overall route and greatly improved final esterification sequence delivered over 2.5 g of EBC-46 (Supplementary Fig. 7). All the steps were performed by two or more investigators to ensure reproducibility. Collectively, our synthetic strategy provides access to B-ring analogues from intermediate **7**, A-ring analogues from intermediates **7–12** and C-ring analogues from intermediate **10**.

Although a comprehensive analysis of the binding, selectivity and biological activities of various analogues will be disclosed separately, it is noteworthy that even modest structural changes dramatically affect PKC affinity and selectivity. To begin our investigation into the role of the C5 $\beta$ -hydroxy-C6 $\alpha$ ,C7 $\alpha$ -epoxy functionality and the C12,C13 esters in determining PKC affinity and selectivity, we prepared an initial series of analogues (Fig. 4a). These analogues, along with EBC-46, were tested for their affinity to PKC- $\beta_1$  and PKC- $\theta$ , representative conventional and novel isoforms of PKC, respectively (Fig. 4b). Specifically, to determine the role of the C6 $\alpha$ ,C7 $\alpha$ -epoxide in PKC binding and selectivity, we synthesized a C6,C7-alkene analogue (**13**, SUW400), otherwise inaccessible from EBC-46.

Interestingly, this analogue exhibited a nearly identical binding affinity and selectivity to PKC- $\beta_1$  and PKC- $\theta$  when compared with that of EBC-46. This finding suggests that the C6 $\alpha$ ,C7 $\alpha$ -epoxide is not necessary for the isoform-selective binding exhibited by EBC-46. Similarly, to determine the role of the C5 $\beta$ -alcohol in the PKC binding and selectivity, we synthesized a C5-deoxy-C6,C7-alkene analogue (**15**, SUW402). This analogue showed a stronger but less selective binding than that of both EBC-46 and SUW400. This finding suggests that the C5 $\beta$ -alcohol plays an important role in isoform binding selectivity. Finally, to begin investigating the role of the C12,C13 esters in PKC binding and selectivity, we synthesized a diacetate analogue (**14**, SUW401). This analogue showed a very low PKC binding affinity when compared with that of EBC-46. This finding suggests that the C12,C13 esters also play an important role in PKC binding. Given the potent PKC affinity of EBC-46, SUW400 and SUW402, these compounds were tested *in vitro* for their ability to permeate CHO-K1 (Chinese hamster ovary factor K1) cells and translocate, in real time, an optically tagged PKC fusion protein (PKC-GFP; GFP, green fluorescent protein) from the cytosol to the membrane—the hallmark of PKC activation<sup>1</sup> (Supplementary Fig. 8). The details and experimental procedures for this assay were published previously<sup>48</sup>. EBC-46 showed a modest translocation of PKC- $\beta_1$ -GFP at low (200 nM) concentrations and a robust translocation at high (1,000 nM) ones (Fig. 4c). Interestingly, the more synthetically accessible SUW400 and SUW402 showed a comparable translocation to that of EBC-46 at low (200 nM) as well as high (1,000 nM) concentrations. Future studies on these and other analogues, readily accessible from our synthetic route, are directed at the elucidation of the structural basis for isoform-selective PKC modulation and the role of isoform selectivity in human immunodeficiency virus and AIDS latency reversal, tumour ablation, antigen enhancement for antigen-targeted antibody and chimeric antigen receptor cell therapies, suppression of T-cell exhaustion and neurological disorders.

In summary, we describe a scalable laboratory preparation of tigilanol tiglate (**1**, EBC-46), an approved veterinary therapeutic and a human clinical lead for cancer and other indications. Previously, tigilanol tiglate was considered synthetically inaccessible and only available from a limited natural source, the latter raising environmental concerns. Our synthetic strategy also enables access to numerous biologically active tiglanes, daphnanes and their analogues. This strategy will accelerate future studies directed at the structural basis for PKC isoform selectivity and its role in mode of action and disease-specific activities.

## Methods

As the hazard of new compounds is unknown, all the procedures were conducted with full personal protective equipment in a way that avoids exposure. CHO-K1 (ATCC) was the cell line used for translocation experiments. No commonly misidentified cell lines were used in this study. None of the cell lines used were authenticated. No statistical methods were used to predetermine sample sizes, but our sample sizes are similar to those reported in previous publications<sup>4</sup>.

## Supplementary Material

Refer to Web version on PubMed Central for supplementary material.

## Acknowledgements

This work was supported by grants from the National Institutes of Health (NIH) (CA31845 and AI124743; Z.O.G., D.J.F., O.D.M., Q.H.L.-N and E.N.). O.D.M. thanks the Molecular Pharmacology Training Program for support. We also thank H. Rahn for thoughtful discussions and assistance in the purification. Confocal images were acquired at the Stanford Neuroscience Microscopy Services. High-resolution mass spectrometric data were acquired at the Vincent Coates Foundation Mass Spectrometry Laboratory, supported in part by NIH P30 CA124435 utilizing the Stanford Cancer Institute Proteomics/Mass Spectrometry Shared Resource. Computational efforts were performed on the Sherlock cluster (Stanford University).

## Data availability

The data supporting the findings of this study are available within the article and its Supplementary Information. The X-ray structure of phorbol-13-acetate bound to the PKC-C1 domain was obtained from the structure reported by Hurley (Protein Data Bank: 1PTR).

## References

1. Newton AC & Brognard J Reversing the paradigm: protein kinase C as a tumor suppressor. *Trends Pharmacol. Sci* 38, 438–447 (2017). [PubMed: 28283201]
2. Kim JT et al. Latency reversal plus natural killer cells diminish HIV reservoir in vivo. *Nat. Commun* 13, 121 (2022). [PubMed: 35013215]
3. Ramakrishna S et al. Modulation of target antigen density improves CAR T-cell functionality and persistence. *Clin. Cancer Res* 25, 5329–5341 (2019). [PubMed: 31110075]
4. Hardman C et al. Synthesis and evaluation of designed PKC modulators for enhanced cancer immunotherapy. *Nat. Commun* 11, 1–11 (2020). [PubMed: 31911652]
5. Marro BS et al. Discovery of small molecules for the reversal of T-cell exhaustion. *Cell Rep.* 29, 3293–3302 (2019). [PubMed: 31801090]
6. Sun M-K, Hongpaisan J, Lim CS & Alkon DL Bryostatin-1 restores hippocampal synapses and spatial learning and memory in adult fragile X mice. *J. Pharmacol. Exp. Ther* 349, 393–401 (2014). [PubMed: 24659806]
7. Kornberg MD et al. Bryostatin-1 alleviates experimental multiple sclerosis. *Proc. Natl Acad. Sci. USA* 115, 2186–2191 (2018). [PubMed: 29440425]
8. Gutiérrez C et al. Bryostatin-1 for latent virus reactivation in HIV-infected patients on antiretroviral therapy. *AIDS* 30, 1385–1392 (2016). [PubMed: 26891037]
9. Farlow MR et al. A randomized, double-blind, placebo-controlled, phase II study assessing safety, tolerability, and efficacy of bryostatin in the treatment of moderately severe to severe Alzheimer's disease. *J. Alzheimers Dis* 67, 555–570 (2019). [PubMed: 30530975]
10. Panizza BJ et al. Phase I dose-escalation study to determine the safety, tolerability, preliminary efficacy and pharmacokinetics of an intratumoral injection of tigilanol tiglate (EBC-46). *EBioMedicine* 50, 433–441 (2019). [PubMed: 31810818]
11. Cullen JK et al. Activation of PKC supports the anticancer activity of tigilanol tiglate and related epoxytiglanes. *Sci Rep.* 11, 1–14 (2021). [PubMed: 33414495]
12. Miller J et al. Dose characterization of the investigational anticancer drug tigilanol tiglate (EBC-46) in the local treatment of canine mast cell tumors. *Front. Vet. Sci* 6, 1–10 (2019). [PubMed: 30723724]
13. Moses RL et al. Novel epoxy-tiglanes stimulate skin keratinocyte wound healing responses and re-epithelialization via protein kinase C activation. *Biochem. Pharmacol* 178, 114048 (2020). [PubMed: 32446889]



14. Boyle GM et al. Intra-lesional injection of the novel PKC activator EBC-46 rapidly ablates tumors in mouse models. *PLoS ONE* 9, 1–12 (2014).
15. FDA Approves First Intratumoral Injection to Treat Non-Metastatic Mast Cell Tumors in Dogs <https://www.fda.gov/news-events/press-announcements/fda-approves-first-intratumoral-injection-treat-non-metastatic-mast-cell-tumors-dogs> (2020).
16. De Ridder TR et al. Randomized controlled clinical study evaluating the efficacy and safety of intratumoral treatment of canine mast cell tumors with tigilanol tiglate (EBC-46). *J. Vet. Intern. Med* 35, 415–429 (2020). [PubMed: 32542733]
17. Lamont RW, Conroy GC, Reddell P & Ogbourne SM Population genetic analysis of a medicinally significant Australian rainforest tree, *Fontainea Picrosperma* C.T. White (*Euphorbiaceae*): biogeographic patterns and implications for species domestication and plantation establishment. *BMC Plant Biol.* 16, 1–12 (2016). [PubMed: 26728271]
18. Grant EL et al. Floral attraction and flower visitors of a subcanopy, tropical rainforest tree, *Fontainea Picrosperma*. *Ecol. Evol* 11, 10468–10482 (2021). [PubMed: 34367589]
19. Paul I, Reddell W, Gordon VA Tiglien-3-one derivatives. US Patent 9770431B2 (2017).
20. Grant E Reproductive Biology, Flowering and Genetics of *Fontainea picrosperma* (*Euphorbiaceae*). PhD thesis, Univ. Sunshine Coast (2020).
21. Wender PA, Quiroz RV & Stevens MC Function through synthesis-informed design. *Acc. Chem. Res* 48, 752–760 (2015). [PubMed: 25742599]
22. Wang Z & Hui C Contemporary advancements in the semi-synthesis of bioactive terpenoids and steroids. *Org. Biomol. Chem* 19, 3791–3812 (2021). [PubMed: 33949606]
23. Wender PA, Verma VA, Paxton TJ & Pillow TH Function-oriented synthesis, step economy, and drug design. *Acc. Chem. Res* 41, 40–49 (2008). [PubMed: 18159936]
24. Kim KE, Kim AN, McCormick CJ & Stoltz BM Late-stage diversification: a motivating force in organic synthesis. *J. Am. Chem. Soc* 143, 16890–16901 (2021). [PubMed: 34614361]
25. Newman DJ & Cragg GM Natural products as sources of new drugs over the nearly four decades from 01/1981 to 09/2019. *J. Nat. Prod* 83, 770–803 (2020). [PubMed: 32162523]
26. Liu WC, Gong T & Zhu P Advances in exploring alternative Taxol sources. *RSC Adv.* 6, 48800–48809 (2016).
27. Wender PA, Rice KD & Schnute ME The first formal asymmetric synthesis of phorbol. *J. Am. Chem. Soc* 119, 7897–7898 (1997).
28. Lee K & Cha JK Formal synthesis of (+)-phorbol. *J. Am. Chem. Soc* 123, 5590–5591 (2001). [PubMed: 11389648]
29. Kawamura S, Chu H, Felding J & Baran PS Nineteen-step total synthesis of (+)-phorbol. *Nature* 532, 90–93 (2016). [PubMed: 27007853]
30. Wang HB, Wang XY, Liu LP, Qin GW & Kang TG Tiglane diterpenoids from the *Euphorbiaceae* and *Thymelaeaceae* families. *Chem. Rev* 115, 2975–3011 (2015). [PubMed: 25906056]
31. Ahmed WA & Salimon J Phorbol ester as toxic constituents of tropical *Jatropha curcas* seed oil. *Eur. J. Sci. Res* 31, 429–436 (2009).
32. Pagani A, Gaeta S, Savchenko AI, Williams CM & Appendino G An improved preparation of phorbol from croton oil. *Beilstein J. Org. Chem* 13, 1361–1367 (2017). [PubMed: 28781702]
33. Zimmermann T, Franzyk H & Christensen SB Phorbol rearrangements. *J. Nat. Prod* 81, 2134–2137 (2018). [PubMed: 30216064]
34. Hou Z, Yao G & Song S Daphnane-type diterpenes from genus *Daphne* and their anti-tumor activity. *Chin. Herbal Medicines* 13, 145–156 (2021).
35. Zhang G, Kazanietz MG, Blumberg PM & Hurley JH Crystal structure of the Cys2 activator-binding domain of protein kinase C $\delta$  in complex with phorbol ester. *Cell* 81, 917–924 (1995). [PubMed: 7781068]
36. Wender PA, Donneley AC, Loy BA, Near KE, Staveness D in *Natural Products in Medicinal Chemistry* (ed. Hanessian S) 475–544 (Wiley-VCH, 2014).
37. Schmidt R & Hecker E Autoxidation of phorbol esters under normal storage conditions. *Cancer Res.* 35, 1375–1377 (1994).

38. Amin HIM et al. The allylic oxidation of tiglane esters. *Fitoterapia* 148, 104802 (2021). [PubMed: 33309651]
39. Ghogare AA & Greer A Using singlet oxygen to synthesize natural products and drugs. *Chem. Rev* 116, 9994–10034 (2016). [PubMed: 27128098]
40. Sagadevan A, Hwang KC & Su M-D Singlet oxygen-mediated selective C—H bond hydroperoxidation of ethereal hydrocarbons. *Nat. Commun* 8, 1812 (2017). [PubMed: 29180784]
41. Lévesque F & Seeberger PH Highly efficient continuous flow reactions using singlet oxygen as a ‘green’ reagent. *Org. Lett* 13, 5008–5011 (2011). [PubMed: 21879739]
42. Volchkov I & Lee D Recent developments of direct rhenium-catalyzed [1,3]-transpositions of allylic alcohols and their silyl ethers. *Chem. Soc. Rev* 43, 4384–4394 (2014).
43. Morrill C, Beutner GL & Grubbs RH Rhenium-catalyzed 1,3-isomerization of allylic alcohols: scope and chirality transfer. *J. Org. Chem* 71, 7813–7825 (2006). [PubMed: 16995691]
44. Ferrier RJ & Hall DW One-step synthesis of glycosidic spiroketals from 2,3-epoxybutyl glycoside derivatives. *J. Chem. Soc. Perkin Trans* 1992, 3029–3034 (1992).
45. Wender PA et al. Gateway synthesis of daphnane congeners and their protein kinase C affinities and cell-growth activities. *Nat. Chem* 3, 615–619 (2011). [PubMed: 21778981]
46. Boudreault PL, Mattler JK & Wender PA Studies on the regio- and diastereo-selective epoxidation of daphnanes and tiglianes. *Tetrahedron Lett.* 56, 3423–3427 (2015). [PubMed: 26034334]
47. Johnson TC et al. Synthesis of Eupalinilide E, a promoter of human hematopoietic stem and progenitor cell expansion. *J. Am. Chem. Soc* 138, 6068–6073 (2016). [PubMed: 27096704]
48. Benner NL et al. Functional DNA delivery enabled by lipid-modified charge-altering releasable transporters (CARTs). *Biomacromolecules* 19, 2812–2824 (2018). [PubMed: 29727572]



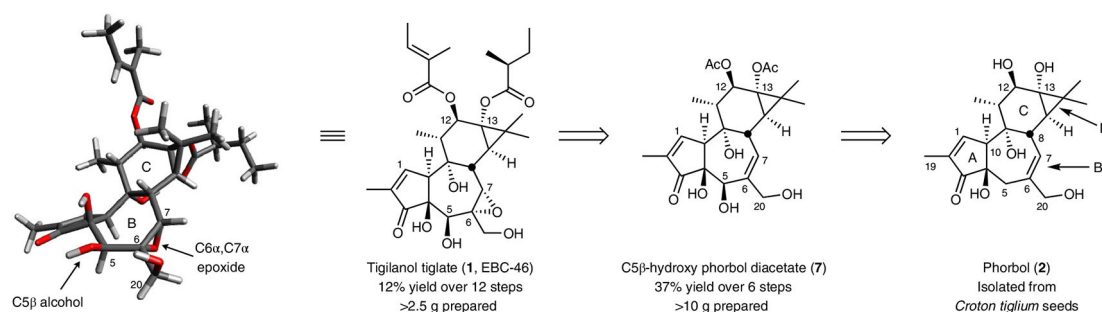


**Fig. 1 l. Structural analysis of tigilanol tiglate (1) and a retrosynthetic analysis of its synthesis from phorbol (2).**

Over 10 g of diversifiable intermediate **7** was prepared from phorbol (**2**), which was isolated in decagram quantities from *C. tiglium* seeds. The three-dimensional structure of **1** was calculated using MacroModel (Schrödinger Suite 2016) and optimized with density functional theory (M06-2X<sup>3</sup>).

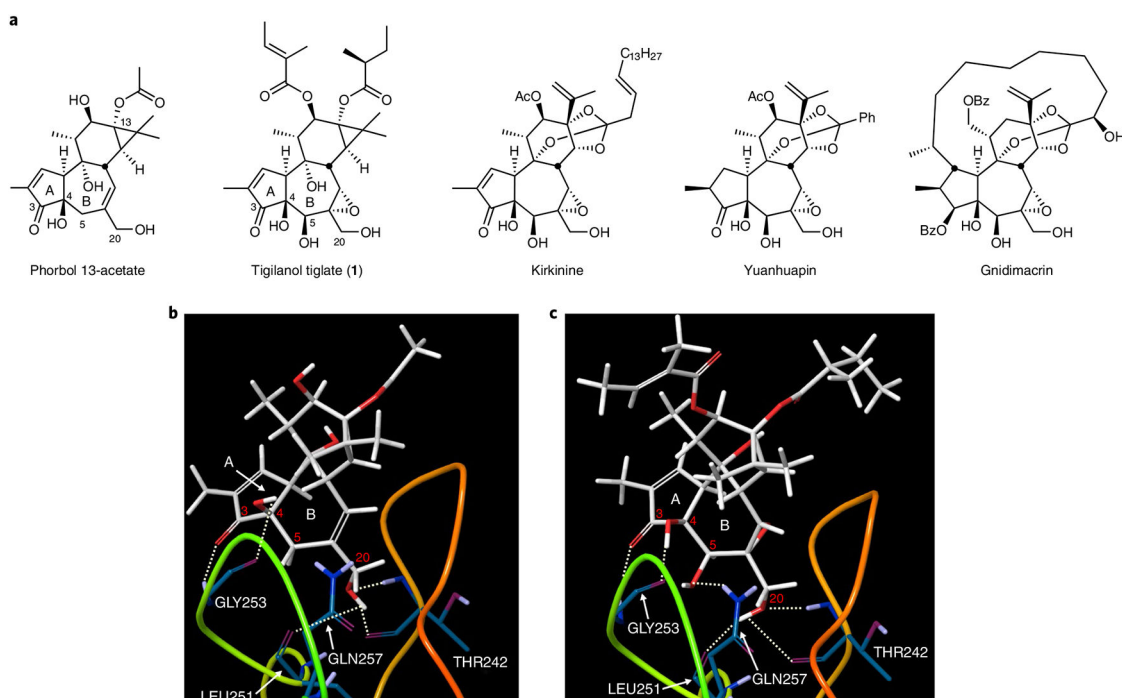


**Fig. 2 |. Overview of the importance of the B-ring oxidation pattern in tigiane and daphnane natural products and the pharmacophore model.**

**a**, The structures of phorbol 13-acetate and of representative members of the tigiane and daphnane families with a shared B-ring functionality. **b**, X-ray crystal structure of phorbol 13-acetate bound to the C1 domain of PKC- $\delta$ <sup>35,36</sup>. **c**, Predicted binding mode of EBC-46 to the C1 domain of PKC- $\delta$ . Dotted lines represent hydrogen bonds.

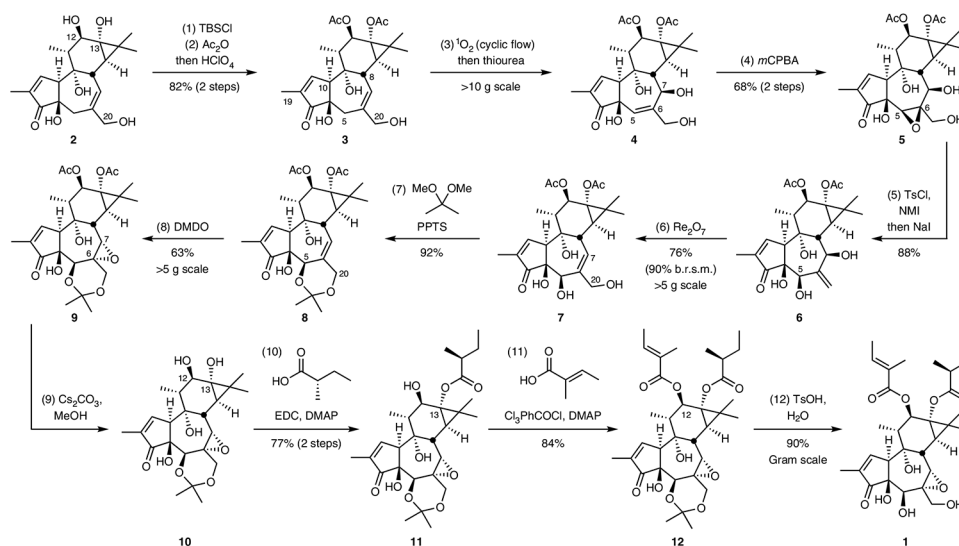


**Fig. 3 |. Reaction sequence from phorbol (2) to tiglanol tiglate (1).**

Reagents and conditions. (1) C20 silylation: *tert*-butyldimethylsilyl chloride (TBSCl) (7 equiv.), imidazole (15 equiv.), dimethylformamide, 0 °C. (2) C12,C13 acetylation and C20 desilylation: acetic anhydride (Ac<sub>2</sub>O) (15 equiv.), triethylamine (NEt<sub>3</sub>) (15 equiv.), 4-dimethylaminopyridine (0.3 equiv.), CH<sub>2</sub>Cl<sub>2</sub>; then MeOH, 0 °C to room temperature; then HClO<sub>4</sub> (25 equiv.). (3) C7 singlet oxygen ene reaction (cyclic flow, approximately 100 cycles of 5 min, reaction progress tracked by thin-layer chromatography and/or NMR spectroscopy; for more information, see Supplementary pages SI-13 and SI-14.); Rose bengal (1.5 mM), O<sub>2</sub>, CD<sub>3</sub>OD, 20 °C; then thiourea (3 equiv.). (4) C5,C6 epoxidation: *m*CPBA (2 equiv.), 3:1 CH<sub>2</sub>Cl<sub>2</sub>:ether, 4 °C. (5) C20 tosylation and reductive epoxide opening: *p*-toluenesulfonyl chloride (TsCl) (1.2 equiv.), NMI (0.1 equiv.), NEt<sub>3</sub> (1.5 equiv.), acetonitrile, 0 °C; then H<sub>2</sub>O; then sodium iodide (NaI) (3 equiv.), 60 °C. (6) C7,C20 allylic transposition: rhenium(VII) oxide (Re<sub>2</sub>O<sub>7</sub>), (0.10 equiv.), THF, 4 °C. (7) C5,C20 acetonide protection: 2,2-dimethoxypropane (300 equiv.), pyridinium *p*-toluenesulfonate (PPTS) (0.15 equiv.), acetone; then rotovap; then acetone (8) C6,C7 epoxidation: dimethyldioxirane (DMDO) (3 equiv.), acetone. (9) C12,C13 deacetylation: Cs<sub>2</sub>CO<sub>3</sub> in methanol (pH = 11). (10) C13 esterification: (*S*)-2-methylbutanoic acid (3 equiv.), 1-ethyl-3-(3-dimethylaminopropyl) carbodiimide (EDC) (3.15 equiv.), NEt<sub>3</sub> (3.30 equiv.), 4-dimethylaminopyridine (DMAP) (0.2 equiv.), CH<sub>2</sub>Cl<sub>2</sub>. (11) C12 esterification: tiglic acid (2.2 equiv.), 2,4,6-trichlorobenzoyl chloride (Yamaguchi reagent) (2 equiv.), NEt<sub>3</sub> (4 equiv.), DMAP (2.6 equiv.), toluene. (12) C5,C20 acetonide deprotection: *p*-toluenesulfonic acid in water (1 M), acetonitrile. b.r.s.m., based on recovered starting material.

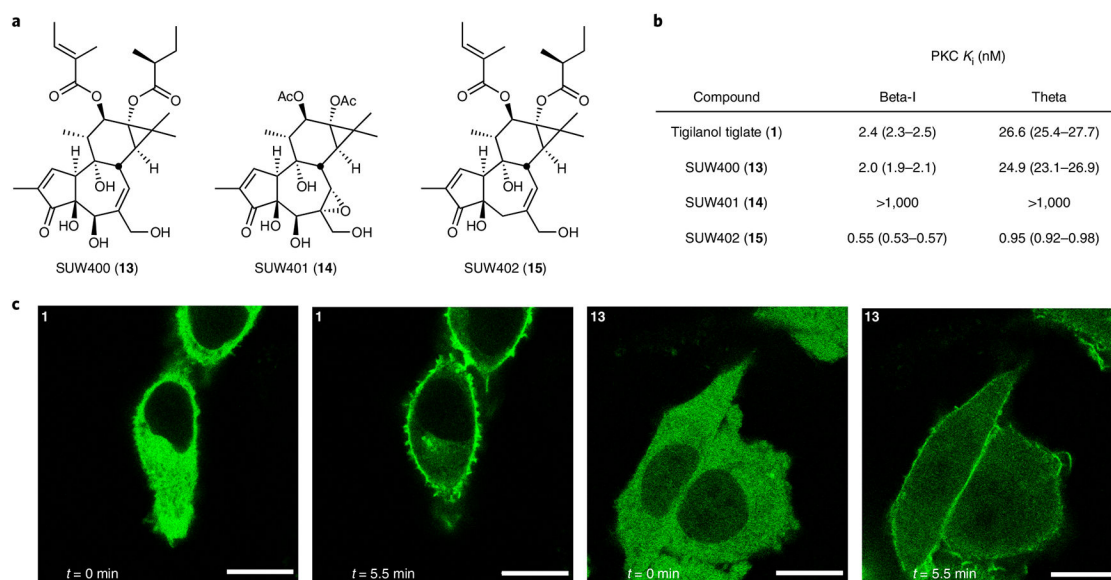


**Fig. 4 |. Representative biological data for synthetic EBC-46 and its analogues.**

**a**, Structures of EBC-46 analogues. **b**, Cell-free PKC binding data for **1**, **13**, **14** and **15**.

The unique PKC $\beta$ -selective binding mode of **1** is mimicked by **13**, whereas **14** exhibits no meaningful PKC binding and **15** binds in a potent and unselective fashion. **c**, In-vitro PKC- $\beta$ I-GFP translocation in CHO-K1 cells mediated by **1** and **13** (1,000 nM). Scale bars, 10  $\mu$ m). Upon exposure to PKC modulators **1** and **13** for 5 min, the GFP-labelled PKC was observed to translocate from the middle of the cells (cytosol) to the periphery (cell membrane).